An experimental comparison of several non linear controllers for power converters[a]

Gerardo Escobar
HEUDIASYC, URA CNRS 817
Université de Technologie de Compiègne
BP 649, 60200 Compiegne, FRANCE
e-mail: escobar@hds.univ-compiegne.fr

Romeo Ortega
Laboratoire des Signaux et Systèmes
CNRS-SUPELEC, UMR CNRS 16
91192, Gif sur Yvette, FRANCE
e-mail: rortega@lss.supelec.fr

Hebertt Sira–Ramirez
Departamento Sistemas de Control
Escuela de Ingeniería de Sistemas
Universidad de Los Andes
Mérida,Venezuela
e-mail: isira@ing.ula.ve

Jean Paul Vilain, Ismail Zein
Laboratoire d'Electrotechnique
Université de Technologie de Compiègne
Centre de Recherches de Royallieu
BP 649, 60200 Compiegne, FRANCE

February 6, 1997

Abstract

In this paper we present an experimental comparative study of five controllers for boost dc–to–dc converters recently reported in the control literature. The controllers are obtained using differents approaches and assumptions on the converter model. They all enjoy some provable stability properties, which are briefly recalled in the paper. To carry out the experiments we constructed a low cost electronic card, which captures the essential features of a commercial product, but with all the sensors required to monitor the behaviour of the system. The algorithms are compared with respect to ease of implementation, in particular their sensitivity to the tuning parameters, and closed–loop performance. The latter is evaluated with the standard criteria of steady–state and transient behaviour, and disturbance attenuation. Motivated by the experimental evidence we propose several modifications to the basic schemes, for some of them we establish some new theoretical results.

A control theorist's first instinct in the face of a new problem is to find a way to use the tools he knows, rather that a commitment to understand the underlying phenomenon. This is not the failure of individuals but the failure of our profession to foster the development of experimental control science. In a way, we have become the prisoners of our rich inheritance and past successes

Y. C. Ho (1982)

[a]This work was supported in part by the Consejo Nacional de Ciencia y Tecnología of Mexico.

1 Introduction

The regulation of switched power converters is a very active area of research both in power electronics and automatic control theory. A typical example of this kind of devices, that captures the essence of the problem, is the boost DC–DC converter. This circuit is described by a bilinear second order model with a binary input. The control task is further complicated by the fact that, with respect to the output to be regulated, the model is nonminimum phase. Boost converters are usually regulated with simple linear lead lag compensators designed using the averaged linear approximation of the model. There is an obvious hard constraint on the achievable performance of this class of controllers, and it is just natural to ask if performance can be improved with nonlinear control. Many theoretical papers in the nonlinear control literature have been devoted to this problem recently. For must of these algorithms we can establish some stability properties. However, it is difficult to assess the merits and drawbacks of these schemes, and in particular the potential performance improvement with respect to the linear designs, based solely on the theoretical analysis.

This paper summarizes the results of an experimental comparison of nonlinear control algorithms on a DC-DC power converter of the boost type. We compare five algorithms, including the linear design, with respect to their ease of implementation and their closed–loop performance. For all these algorithms local asymptotic stability of the desired equilibrium is insured. The motivation of the present study is not to illustrate the validity of these theoretical results, but to test their performance when confronted with situations not predicted by the theory. The behaviour of the schemes is compared with the following basic criteria: transient and steady state response to steps and sinusoidal references, attenuation of disturbances in the power supply and sensitivity to unknown loads. Particular emphasis is placed throughout the paper on the flexibility provided by the tuning parameters to shape the responses. Eventhough this issue is not always appreciated in theoretical studies, we have found it of prime importance in experimentation.

The rest of the paper is organized as follows: in section 2 we introduce the model of the boost circuit. In section 3 we present the five differents strategies to be studied. Their adaptive versions, when applicable, are given in section 4. In section 5 we give a brief description of the experimental set-up. In section 6 we present the experimental results. We finish this article with our conclusions in section 7.

2 Switch-regulated boost converter

In this section we first give the boost converter circuit with its exact and approximate descriptions. Then, we present some system–theoretic properties of these models which are exploited in the control designs.

2.1 Exact and averaged model

Throughout the paper we consider the switch–regulated "boost" converter circuit of figure 1.

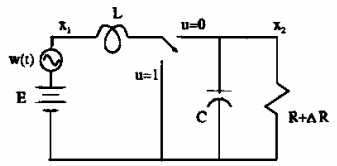

Figure 1: Switch- regulated Boost circuit

The differential equations describing the circuit are given by

$$\begin{aligned} \dot{x}_1 &= -(1-u)\frac{1}{L}x_2 + \frac{E+\omega}{L} \\ \dot{x}_2 &= (1-u)\frac{1}{C}x_1 - \frac{1}{(R+\Delta R)C}x_2 \end{aligned} \tag{1}$$

where x_1 and x_2 represent, respectively, the input inductor current and the output capacitor voltage variables; $E > 0$ represents the nominal constant value of the external voltage source and ω is an unknown (time varying) disturbance, which satisfies $|\omega| < E$; R represents the nominal constant value of the output resistance and ΔR reflects the parametric uncertainty; u, which takes values in the discrete set $\{0, 1\}$, denotes the switch position function, and acts as a control input. The regulated output is x_2 which should be driven to some constant desired value $V_d > E$.

The control laws that we consider are classified into two groups depending on whether they generate directly the switching signal u, or they require an auxiliary Pulse Width Modulation (PWM) circuit to determine the switch position. In the latter case the PWM policy is specified as follows,

$$u(t) = \begin{cases} 1 & \text{for} \quad t_k \le t < t_k + \mu(t_k)T \\ 0 & \text{for} \quad t_k + \mu(t_k)T \le t < t_k + T \end{cases}$$

where t_k represents a sampling instant defined by $t_{k+1} = t_k + T$, $k = 0, 1, \ldots$; the parameter $T > 0$ is the fixed sampling period, also called the duty cycle. The duty ratio function, $\mu(\cdot)$, ranging on the closed interval $[0, 1]$, is now the control input to the PWM device.

While the first class of controllers directly proceeds from the exact (hybrid) description (1), the control algorithms that use a PWM policy are designed based on an approximate (continuous–time) averaged model [9], [13], which is given by

$$\begin{aligned} \dot{z}_1 &= -(1-\mu)\frac{1}{L}z_2 + \frac{E+\omega}{L} \\ \dot{z}_2 &= (1-\mu)\frac{1}{C}z_1 - \frac{1}{(R+\Delta R)C}z_2 \end{aligned} \tag{2}$$

where we denote by z_1 and z_2 the average input current and the average output capacitor voltage, respectively. As discussed in [13] this model accurately describes the behaviour of the converter provided the switching is sufficiently fast and the capacitor voltage is bounded away from zero, i.e., $x_2 \ge \epsilon > 0$. Notice that the only difference between the two models is that now μ is a continuous, and not a binary, signal.

For ease of reference we will be using the following, more compact, matrix representation of the averaged model (2),

$$\mathcal{D}\dot{z} - (1-\mu)\mathcal{J}z + \mathcal{R}z = \mathcal{E} \tag{3}$$

where

$$\mathcal{D} = \begin{bmatrix} L & 0 \\ 0 & C \end{bmatrix} \quad ; \quad \mathcal{J} = \begin{bmatrix} 0 & -1 \\ 1 & 0 \end{bmatrix} \quad ; \quad \mathcal{R} = \begin{bmatrix} 0 & 0 \\ 0 & \frac{1}{R+\Delta R} \end{bmatrix} \quad ; \quad \mathcal{E} = \begin{bmatrix} E+\omega \\ 0 \end{bmatrix} \tag{4}$$

With the exception of the section on experimental results, throughout the paper we consider only the nominal model, hence we take $\Delta R \equiv 0$, $\omega \equiv 0$.

2.2 Control properties

Control of the boost converter is a challenging problem because, besides being a bilinear system, –with a binary input in its exact description, or a saturated one in the averaged model–, it is also a non–minimum phase system with respect to the output to be controlled [13]. The existence of unstable zero dynamics puts a hard constraint on the achievable performance [3], a fact which is well known in the power electronics community [6]. It also considerably complicates the task of designing a nonlinear controller, since must existing techniques rely (in one way or another) on stable invertibility of the plant.

Fortunately, the non–minimum phase obstacle can be overcomed noting that, with respect to the inductor current, it is a minimum–phase system, and that there is a one-to-one correspondence between the output voltage and the inductor current equilibria. The voltage is then indirectly controlled via regulation of the current. An important drawback of this approach, that was observed in the experiments, is the high sensitivity to the circuit parameters, in particular to the load resistance. Another fundamental property of the system that is exploited by some of the controllers is that (as expected) the circuit defines a passive mapping from the input voltage E to the inductor current x_1. Roughly speaking, this feature is used in passivity–based schemes to design a controller that preserves passivity in closed–loop. Eventhough all these properties have already been reported in, e.g., [13], we repeat them here for completeness.

Property 1 *(Uniqueness of the equilibrium point)*

For a constant duty ratio $\mu = \overline{\mu} \in (0,1)$, the steady state values of the average input current $\overline{z}_1$ and average output voltage $\overline{z}_2$ of (2) are related by

$$\overline{z}_1 = \frac{\overline{z}_2^2}{ER} \tag{5}$$

Consequently, given a desired value V_d for the average output voltage then the corresponding average input current may be uniquely determined.

□□□

This property follows inmediately from the analysis of the equilibrium point of the averaged model (2), which is readily obtained as,

$$\overline{z}_1 = \frac{E}{R(1-\overline{\mu})^2} \quad ; \quad \overline{z}_2 = \frac{E}{1-\overline{\mu}} \tag{6}$$

Notice that, since $\overline{\mu} < 1$, the average steady–state output voltage $\overline{z}_2$ exceeds the value of the external input source E, revealing the "step–up" character of the circuit.

Property 2 *(Nonminimum phasedness)*

The zero dynamics of (2) with output z_2 are unstable while they are (locally) stable if we take z_1 as the output.

□□□

To prove this fact, consider first the case where the average output capacitor voltage z_2 is regarded as the output of the average PWM model (2). A straightforward elimination of z_1 from the set of differential equations (2) leads to the following nonlinear input–output differential representation,

$$\ddot{z}_2 + \left(\frac{1}{RC} + \frac{\dot{\mu}}{1-\mu}\right) \dot{z}_2 + \frac{1}{LC}\left[(1-\mu)^2 + \frac{L}{R}\frac{\dot{\mu}}{1-\mu}\right] z_2 = (1-\mu)\frac{E}{LC} \tag{7}$$

The "zero dynamics" at an equilibrium point $\overline{z}_2 = V_d$, associated with this input–output representation, is obtained by letting $\dot{z}_2 = 0$ and $\ddot{z}_2 = 0$ (see Fliess [2]). The resulting differential equation describing the "remaining dynamics" of the duty ratio function μ is simply obtained as

$$\dot{\mu} = \frac{R(1-\mu)^2}{LV_d}\left[E - (1-\mu)V_d\right] \tag{8}$$

The equilibrium points of (8) are given by

$$\overline{\mu} = 1 \quad ; \quad \overline{\mu} = 1 - \frac{E}{V_d} \tag{9}$$

with the latter being the only physically relevant. The phase diagram of equation (8), shown in figure 2, readily reveals that this equilibrium point is unstable. We conclude that the average PWM model of the boost converter, with output represented by the average capacitor voltage z_2, is actually a *nonminimum phase* system.

Consider now as output the average input current, z_1. One obtains the following differential input–output representation for the average system

$$\ddot{z}_1 + \left(\frac{1}{RC} + \frac{\dot{\mu}}{1-\mu}\right) \dot{z}_1 + \left[(1-\mu)^2\frac{1}{LC}\right] z_1 = \frac{E}{L}\left(\frac{1}{RC} + \frac{\dot{\mu}}{1-\mu}\right) \tag{10}$$

The "zero dynamics" at an equilibrium point $z_1 = I_d$, associated with the input–output representation (10), is obtained as,

$$\dot{\mu} = \frac{1-\mu}{RCE}\left[(1-\mu)^2 RI_d - E\right] \tag{11}$$

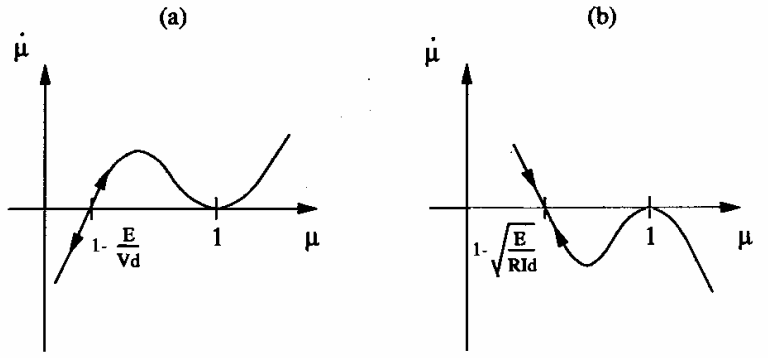

Figure 2: Zero dynamics phase diagram a) Non–minimum phase behaviour, b) Minimum phase behaviour

The equilibrium points of (8) are given by

$$\mu = 1 \quad ; \quad \mu = 1 + \sqrt{\frac{E}{RI_d}}; \quad \mu = 1 - \sqrt{\frac{E}{RI_d}} \tag{12}$$

Again, the latter is the only physically significant point. The phase diagram of equation (11), shown in figure 2, reveals that this equilibrium point is now locally stable. We conclude that the average PWM model of the boost converter, with output represented by the average input inductor current $y = z_1$, is a *minimum phase* system.

We conclude this subsection with the important, though not unexpected, observation that the averaged circuit dynamics (3) defines a passive operator.

Property 3 *(Passivity)*
The boost converter model (3) defines a passive operator $E \to z_1$.

□□□

To establish this fact consider the *total energy* of the average circuit model

$$H = \frac{1}{2} z^T \mathcal{D} z = \mathcal{T}_\mu + \mathcal{V}_\mu \tag{13}$$

with $\mathcal{T}_\mu = \frac{1}{2} L z_1^2$ and $\mathcal{V}_\mu = \frac{1}{2} C z_2^2$ the magnetic co-energy and electric energy, respectively. Then, take the time derivative of H along the trajectories of (3), notice the skew–symmetry of $\mathcal{J}$, and integrate back to get the energy balance equation

$$\underbrace{H(t) - H(0)}_{\text{stored energy}} + \underbrace{\frac{1}{R}\int_0^t z_2^2(\tau)\ \mathrm{d}\tau}_{\text{dissipated energy}} = \underbrace{\int_0^t z_1(\tau) E\ \mathrm{d}\tau}_{\text{supplied energy}}$$

This equation reveals that the "forces" $(1-\mu)\mathcal{J}z$, appearing in (3), are *workless*. Notice that the control action only "transfers" the energy between the inductance and the capacitance, hence it does not affect the energy balance.

3 Control laws

In this subsection we present the five control laws that will be compared in this paper. The first one is a simple state–feedback pole placement scheme based on the first order approximation of the model, which (in the form of lead-lag circuit) is the industry standard [6]. The other schemes are nonlinear and rely on linearization [11], passivization [13], sliding modes [12] and a combination of sliding modes and passivity

[14]. In the absence of external disturbances and parameter uncertainty, i.e., when $\omega \equiv 0, \Delta R \equiv 0$, they all achieve (local) asymptotic stabilization, that is, they insure that for suitable initial conditions $z_2 \to V_d$ with internal stability. We refer the reader to these references for further details on the schemes.

As explained above they are divided into two groups depending on whether they use or not an auxiliary PWM circuit to generate the control signal. This means also that for the control design, they use the continuous (averaged) or the switched (exact) model, respectively. In the lack of a better terminology we use these qualifiers to classify them below.

3.1 Continuous control laws

- **Linear Averaged Controller (LAC)**

This controller is based on the linearization of the averaged model (2) around an equilibrium point (see [16] for more details). Given a desired output volage $\overline{z}_2 = V_d$ the corresponding $\overline{z}_1$ and $\overline{\mu}$ can be uniquely obtained from (5) and (6) as

$$\overline{z}_1 = \frac{V_d^2}{RE} \;\; ; \;\; \overline{z}_2 = V_d \;\; ; \;\; \overline{\mu} = 1 - \frac{E}{Vd}$$

Defining the following error variables

$$\tilde{z}_1 = z_1 - \overline{z}_1 \;\; ; \;\; \tilde{z}_2 = z_2 - \overline{z}_2 \;\; ; \;\; \tilde{\mu} = \mu - \overline{\mu}$$

we write the linearized model as

$$\dot{\tilde{z}} = A\tilde{z} + B\tilde{\mu} \tag{14}$$

where A and B are given by

$$A = \begin{bmatrix} 0 & -\frac{1-\overline{\mu}}{L} \\ \frac{1-\overline{\mu}}{C} & -\frac{1}{RC} \end{bmatrix} = \begin{bmatrix} 0 & -\frac{E}{V_d L} \\ \frac{E}{V_d C} & -\frac{1}{RC} \end{bmatrix}$$

$$B = \begin{bmatrix} \frac{\overline{z}_2}{L} \\ -\frac{\overline{z}_1}{C} \end{bmatrix} = \begin{bmatrix} \frac{V_d}{L} \\ -\frac{V_d^2}{RLC} \end{bmatrix}$$

Some simple calculations show that the pair $(A,\ B)$ is controllable. Hence, the poles of $(A - BK)$ can be located arbitrarily with a suitable choice of the state feedback gains $K = [k_1 \;\; k_2]$.

Now, taking the averaged error voltage as the output we obtain the following transfer function

$$H(s) = \frac{N_1(s)}{D(s)} = \frac{\mathcal{K}(s - \mathcal{Z}_1)}{(s - \mathcal{P}_1)(s - \mathcal{P}_2)} \tag{15}$$

As expected from the discussion of section 2.2 and the commutativity of the operations of linearization and zero dynamics extraction [5], the lincar system has a right hand plane (rhp) zero. The latter is given by

$$\mathcal{Z}_1 = \frac{RE^2}{LV_d^2}$$

while the two stable poles are located in

$$\mathcal{P}_{1,2} = -\frac{1}{2RC}(1 \pm \sqrt{1 - 4\frac{E^2R^2C}{V_d^2 L}}) \tag{16}$$

The system will display an initial undershoot because it has an odd number of real open rhp zeros [8].

If we now take instead as output the averaged error current $\tilde{z}_1$, then we obtain a transfer function as in (15) but with a left half plane zero located in

$$\mathcal{Z} = -\frac{2}{RC}$$

This fact justifies the common practice of using the current to compute the control law for this system, usually called *current* or *indirect* control.

- **Feedback Linearizing Controller (FLC)**

In [11] a nonlinear (static state feedback) controller that linearizes the input-output behaviour of the system, with output the circuit total energy (13), was proposed as follows.

$$\mu = \frac{1}{(\frac{E}{L} + \frac{2}{RC} z_1) z_2} \left\{ \left(\frac{2}{R^2 C} - \frac{a_1}{R} + \frac{a_2 C}{2} \right) z_2^2 + \left(a_1 E + \frac{a_2 L}{2} z_1 \right) z_1 + \frac{E^2}{L} - a_2 H_d \right\} \tag{17}$$

where $a_1, a_2 > 0$ are the design parameters, and

$$H_d := \frac{V_d^2}{2} (C + \frac{L}{R^2 E^2} V_d^2). \tag{18}$$

More precisely, it is shown in [11], that the converters total energy (13) evaluated along the trajectories of the closed–loop system (2), (17), (18) satisfies the linear equation

$$\ddot{H} + a_1 \dot{H} + a_2 H = a_2 H_d \tag{19}$$

Notice that H_d is the energy level required to ensure that as $H \to H_d$ we have $z_2 \to V_d$, as desired. Since the dynamics is now linear, the convergence rate can be fixed arbitrarily with a suitable choice of the controller parameters a_1, a_2.

The advantage of having a linear closed–loop dynamics, expressed in some physically meaningful variables, can hardly be overestimated. It allows us to easily predict the effect of the tuning parameters and simplify the controller commissioning. However, as will be shown by our experiments, the existence of unmodelled nonlinearities, and in particular input saturation, limits the validity of these predictions.

- **Passivity-Based Controller (PBC)**

In [13] the following (nonlinear dynamic) controller that preserves passivity of the closed loop was proposed

$$\mu = -\frac{1}{z_{2d}} \left[E + R_1 \left(z_1 - \frac{V_d^2}{RE} \right) \right] \tag{20}$$

where the controller dynamics is given by

$$\dot{z}_{2d} = -\frac{1}{RC} \left\{ z_{2d} - \frac{V_d^2}{E z_{2d}} \left[E + R_1 \left(z_1 - \frac{V_d^2}{RE} \right) \right] \right\}, \; z_{2d}(0) > 0 \tag{21}$$

where $R_1 > 0$ is a design parameter.

The system (2) in closed loop with the controller (20), (21) is described by

$$\mathcal{D} \dot{\tilde{z}} - (1 - \mu) \mathcal{J} \tilde{z} + \mathcal{R}_d \tilde{z} = 0 \tag{22}$$

where $\tilde{z} = z - [\frac{V_d^2}{RE}, z_{2d}]^T$ and

$$\mathcal{R}_d = \begin{bmatrix} R_1 & 0 \\ 0 & \frac{1}{R} \end{bmatrix}$$

Looking now at the quadratic function $V_d := \frac{1}{2} \tilde{z}^T \mathcal{D} \tilde{z}$, whose derivative satisfies

$$\dot{V}_d = -\tilde{z} \begin{bmatrix} R_1 & 0 \\ 0 & \frac{1}{R} \end{bmatrix} \tilde{z} \leq -\alpha V_d, \quad \alpha := \frac{\min(R_1, \frac{1}{R})}{\max(L, C)} > 0 \tag{23}$$

we see that R_1 injects the damping required for asymptotic stability, and that the convergence rate of $\tilde{z}$ to zero is improved by pumping up R_1. From these observations one might be tempted to try a high-gain design, which a more careful analysis (and our experiments) reveals not to be a good idea. To see this notice that $\tilde{z}_2 \to 0$ does not imply that $z_2 \to V_d$ as desired, unless $z_{2d} \to V_d$ as well. To study the behaviour of the latter consider the signal $\eta := \frac{1}{2}(z_{2d}^2 - V_d^2)$, which satisfies

$$RC \dot{\eta} = -2\eta + \frac{R_1 V_d^2}{E} \tilde{z}_1 \tag{24}$$

This equation clearly shows two important limitations of the scheme: first, that the speed of convergence is essentially determined by the natural time constant of the converter. Remark that even if $\tilde{z}_1$ converges to zero very fast, z_{2d} (and consecuently z_2) evolves with this time constant. Second, that increasing the damping will induce a "peaking" in η, and consequently a slower convergence of $z_{2d} \to V_d$.

Furthermore, we have that even the convergence rate of $\tilde{z}$ is bounded from below by the undamped dynamics, i.e. $\alpha \geq \frac{1}{RC}$. The sluggishness of this scheme has been observed in our experiments. To overcome this drawback we have tried to add some damping in the subsystem asociated to z_{2d}, that is, we modify (21) to

$$\dot{z}_{2d} = -\frac{1}{RC}\left\{ z_{2d} - \frac{V_d^2}{E z_{2d}}\left[E + R_1\left(z_1 - \frac{V_d^2}{RE}\right) + R_2(z_2 - z_{2d})\right]\right\},\ z_{2d}(0) > 0$$

with $R_2 > 0$ the new damping coefficient. This gives a closed–loop of the form (22) but with a new damping matrix

$$\begin{bmatrix} R_1 & 0 \\ 0 & \frac{1}{R} + R_2 \end{bmatrix}$$

Hence the convergence of $\tilde{z}$ to zero can be made arbitrarily fast. Unortunately, this does not change significantly the dynamics of z_{2d}, since η now satisfies

$$RC\dot{\eta} = -2\eta + \frac{V_d^2}{E}(R_1\tilde{z}_1 + R_2\tilde{z}_2)$$

Another possibility is to use cross terms in the damping matrix R_d. All these modifications were tried experimentally but no significant improvement was obtained.

3.2 Switched control laws

- **Sliding Mode Controller (SMC)**

  In [12] the following indirect sliding mode controller is proposed for the exact model (1)

$$u = 0.5\,[\,1 - sgn\ (s)] \tag{25}$$

where

$$s = x_1 - V_d^2/RE$$

is the switching line along the desired current value. It can be shown that this switching policy locally creates a *stable* sliding regime on the line $s = 0$ with ideal sliding dynamics characterized by

$$\overline{x}_1 = \frac{V_d^2}{RE}\ \ ;\ \ \dot{\overline{x}}_2 = -\frac{1}{RC}\left[\overline{x}_2 - \frac{V_d^2}{\overline{x}_2}\right]\ \ ;\ \ u_{eq} = 1 - \frac{E}{\overline{x}_2} \tag{26}$$

Moreover, the ideal sliding dynamics behaviour of the capacitor voltage variable, described by (26), can be explicitly computed as

$$\overline{x}_2(t) = \sqrt{V_d^2 + \left[\overline{x}_2^2(t_h) - V_d^2\right] e^{-\frac{2}{RC}(t-t_h)}} \tag{27}$$

where t_h stands for the reaching instant of the sliding line $s = 0$.

This result can be easy explained as follows. Suppose we take the value of zero as the initial condition for the capacitor voltage x_2, this will remain zero, while the switch position u is maintained at the value $u = 1$. The inductor current grows, during this "reaching" phase as a linear function of time

$$x_1(t) = \frac{E}{L}\,t \tag{28}$$

When the sliding line $s = x_1 - V_d^2/RE = 0$ is reached at time $t_h = (L/R)(V_d/E)^2$, the voltage capacitor x_2 grows from zero towards its equilibrium value V_d, ideally governed by

$$\overline{x}_2(t) = V_d\sqrt{1 - e^{-\frac{2}{RC}(t-t_h)}} \tag{29}$$

Notice that, similarly to **PBC**, it is the open–loop time constant that regulates this dynamics. Furthermore, we will show in our experiments that this remarkably simple approach is, unfortunately, extremely sensitive

to parameter uncertainty and noise. Finally, as usual with sliding mode strategies, the energy consumption is very high.

- **Sliding Mode plus Passivity Based Controller (SM+PBC)**

To try to reduce the energy consumption in the latter scheme we proposed in [14] to combine sliding modes with passivity. The switching policy is now given by

$$u = 0.5[1 - sgn\ (s)] = 0.5[1 - sgn\ (x_{1d} - V_d^2/RE)\ ] \tag{30}$$

with the controller dynamics given by

$$\begin{aligned} \dot{x}_{1d} &= -\frac{1}{L}(1-u)x_{2d} + \frac{R_1}{L}(x_1 - x_{1d}) + \frac{E}{L} \\ \dot{x}_{2d} &= \frac{1}{C}(1-u)x_{1d} - \frac{1}{RC}x_{2d} \end{aligned} \tag{31}$$

Notice that we take now as the switching line $s = x_{1d} - V_d^2/RE$, where x_{1d} evolves according to the dynamics (31). The latter being a copy of the open–loop dynamics to which we have added damping via R_1.

For this new control policy we can also prove that it locally creates a sliding regime on the line $s = 0$. Moreover, the converter state trajectory x converges towards the auxiliary state trajectory x_d and, in turn, x_d converges towards the desired equilibrium state, i.e.,

$$(x_1, x_2) \rightarrow (x_{1d}, x_{2d}) \rightarrow \left(\frac{V_d^2}{RE}, V_d\right)$$

To assess the performance enhancement of **SM+PBC** it is shown in [14] that while under **SMC** the performance index

$$\int_0^\infty H(\tau)\ \mathrm{d}\,\tau = \int_0^\infty \frac{1}{2}\left[L\left(x_1(\tau) - \frac{V_d^2}{RE}\right)^2 + C\,(x_2(\tau) - V_d)^2\right]\ \mathrm{d}\,\tau \tag{32}$$

is unbounded for all initial conditions, it remains finite with **SM+PBC** (provided we choose the controller initial values satisfying $x_{1d}(0) \neq x_1(0)$ and $x_{2d}(0) \leq V_d$).

Consistent with the statement above, our experiments will show that the as the initial conditions for the controller are chosen "closer" to the desired equilibrium state of the controlled plant, the state responses of the plant become smoother with slightly larger settling times but with a much better behaved transient shape. Unfortunately, it suffers from the same drawback as **PBC** of providing no freedom to shape the response of the output voltage.

4 Modified control laws

All the control strategies presented above are of the indirect type, where we control the capacitor voltage via regulation of the inductor current and invoke the one-to-one corresponence between their equilibria to achieve the output regulation objective. This strategy is clearly very sensitive to parameter uncertainty, in particular load resistance changes. To overcome this drawback we have tried two different modifications to the control laws, the simple addition of an integral loop around the voltage error, and the incorporation of an adaptation mechanism. For the former we do not dispose of any theory to assess the stability of the closed loop, while for the latter a complete stability analysis can be performed. Interestingly enough, in some of our experiments the integral action provided a more satisfactory performance than the full-blown adaptive schemes.

4.1 Adaptive schemes

- **Adaptive PBC**

In [15] we proposed the following *adaptive* version of the **PBC**

$$\mu = 1 - \frac{1}{z_{2d}}\left[E + R_1\left(z_1 - \hat{\theta}\frac{V_d^2}{E}\right) + L\frac{V_d^2}{E}\gamma z_{2d}\left(z_2 - z_{2d}\right)\right] \tag{33}$$

with controller auxiliar dynamics given by

$$\dot{z}_{2d} = -\frac{\hat{\theta}}{C}\left\{z_{2d} - \frac{V_d^2}{z_{2d}E}\left[E + R_1\left(z_1 - \hat{\theta}\frac{V_d^2}{E}\right) + L\frac{V_d^2}{E}\gamma z_{2d}\left(z_2 - z_{2d}\right)\right]\right\} \tag{34}$$

being the parameter $\hat{\theta}$ the estimate of $\frac{1}{R}$, which is updated with the following adaptive law

$$\dot{\hat{\theta}} = -\gamma z_{2d}\left(z_2 - z_{2d}\right) \tag{35}$$

$\gamma > 0$ is a designer chosen constant that fixes the adaptation speed. It is shown in [15] that the system (2) in closed loop with the controller (33) has an equilibrium point given by,

$$(z_1, z_2, z_{2d}, \hat{\theta}) = \left(\frac{V_d^2}{RE}, V_d, V_d, \frac{1}{R}\right) \tag{36}$$

which is *asymptotically stable*.

To understand the rationale of this scheme compare (33), (34) with its nonadaptive version (20), (21). The former is obtained replacing in the latter $\frac{1}{R}$ by its estimate and adding inside the square bracketts in both equations a term proportional to $\dot{\hat{\theta}}$. The need for this term, which makes the scheme different from a "certainty–equivalent" version, is related with a relative degree problem in the stability analysis.

- **Adaptive SMC**

To add adaptation to the basic **SMC** we propose to modify the switching line as

$$s = x_1 - \hat{\theta}\frac{V_d^2}{E}$$

with the parameter $\hat{\theta}$ estimated by

$$\dot{\hat{\theta}} = -\gamma V_d\left(x_2 - V_d\right), \quad \gamma < \frac{E^2}{V_d^4 L} \tag{37}$$

To understand the rationale behind this scheme, note that in the switching line, the term $1/R$ has been replaced by its estimation $\hat{\theta}$. Moreover, the adaptation law (37) was motivated by the form of the corresponding adaptive version for the case PBC where z_{2d} has been substituted by V_d, this because now we don't have any auxiliary dynamics as before.

- **Adaptive SM+PBC**

An adaptive version for the **SM+PBC** can be similarly obtained considering the same switching line as above, but using the estimator

$$\dot{\hat{\theta}} = -\gamma x_{2d}\left(x_2 - x_{2d}\right) \tag{38}$$

The controller auxiliary dynamics is modified accordingly to

$$\begin{aligned} \dot{x}_{1d} &= -\frac{1}{L}(1-u)x_{2d} + \frac{R_1}{L}(x_1 - x_{1d}) + \frac{E}{L} \\ \dot{x}_{2d} &= \frac{1}{C}(1-u)x_{1d} - \frac{\hat{\theta}}{C}x_{2d} \end{aligned} \tag{39}$$

Again, the rationale behind this scheme is to substitute $1/R$ by its estimated value $\hat{theta}$ whenever it occurs, and take the form of the adaptive law to estimate this value as in the PBC case (35), but now using x_2, x_{2d} instead of z_2, z_{2d}, respectively.

4.2 Adding an integral term

In all our experiments we have observed the presence of steady state errors in the output. This is due to the existence of dynamics in the real circuit, associated to parasitics appearing in the electronic and passive elements, which are not considered in the model. Of course, this error is further accentuated when we perturb the load resistance. Experimentally we have seen that adding an integral term to the control law we could compensate this error or make it negligible, such an integral term can be computed in the following way

$$-K_i \int_0^t [x_2(s) - V_d] ds \quad ; \quad K_i > 0$$

Note that this term is continuous so we can add it only to the duty ratio $\mu(t)$ which is also a continuous function, this implies that we can only apply it to the three laws using the averaged model, i.e., **LAC**, **FLC** and **PBC**.

5 Experimental configuration

The experimental card was assembled using low cost commercial electronic elements placed on a card designed in the laboratory. In fig. 3 we show the experimental set-up consisting of the boost circuit card that receives control signals from a D/A converter of a DSpace card placed in a PC. The DSpace card acquires, using an A/D converter, the output voltage and inductor current signals previously conditioned from the boost card. Two DC power supplies are necesary to operate the whole system, one to provide energy to the boost system (we will refer to it as the power supply in the rest of the paper), and the other one to feed the electronic part of the card.

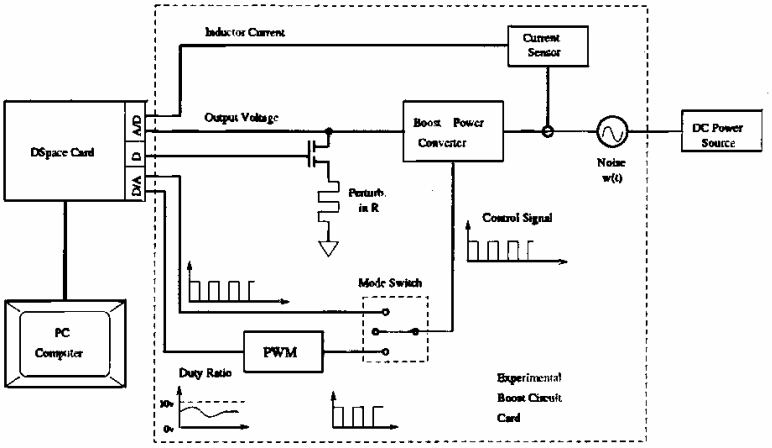

Figure 3: Experimental set-up

In fig. 4 we show the main card which is formed by a boost circuit, a pulse width modulation circuit (PWM), and some signal conditioners. This design is very close to that of [4].

The boost circuit is basically composed by an inductor, a capacitor, a resistive charge and a switch, the last one is implemented by interconecting a FET transistor and a rapid diode in a suitable maner, all this elements feeded by a DC power supply. The values of its elements are shown below.

Element	Value	Unities
Capacitance	1000	μF
Inductance	170	mH
Resistance	100	Ω
Power supply	10	$Volt$

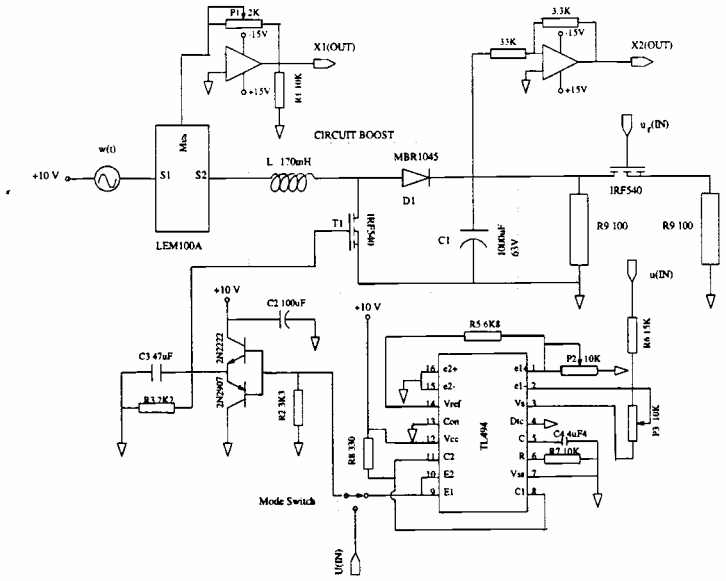

Figure 4: Boost circuit card

A current sensor together with a current to voltage converter are introduced to make available the inductor current x_1. In this way, in form of a voltage signal we can feed it into the DSpace card to be used in the control law. In the case of the output voltage x_2 we put a voltage divisor so we can reduce the level of this signal in such a way that its final value is always in the range [0,10] Volts. To compensate the nonlinear characteristic of the current sensor and some offset introduced by the linear amplifier circuits, we computed their characterisic functions and implemented their inverse.

In this card we have the choice between controlling the boost circuit by means of a PWM generated signal or by directly introducing a switching signal coming from the DSpace card. This selection is done depending on the position of the *mode switch*. If a PWM control is selected, then we should feed a continuous signal that represents the duty ratio in the range $[0, 10]$ Volts corresponding to $[0, 100]\%$. The PWM circuit was designed using a commercial integrated circuit and it was programmed to have a sampling rate of 50 KHz. On the other hand, if switched control is selected, then we should provide a switching signal going from 0 to 5 Volts.

Another interesting feature of the card is the possibility to connect or disconnect another resistive charge in parallel to the output by means of a digital output signal coming from the DSpace card that commands the gate of a MOSFET acting as a switch.

To study the effect of disturbances in the power source w, a driver circuit has been interconected between the power supply and the boost circuit. In this way we can introduce disurbance signals from a signal generator or even from the PC.

Programs are written in a PC using C language. The programs containing the description of the controllers are translated and down-loaded into the DSpace memory as assembler programs by means of a suitable software. Time derivatives in some of the control laws are discretized using a rectangular aproximation with a sampling period of 6×10^{-5} sec.

6 Experimental results

The five control laws described in the previous section have been implemented in the above boost circuit card. Their behaviour is compared with the following basic criteria:

i) transient and steady state response to steps and sinusoidal output voltage references,

ii) attenuation of step and sinusoidal disturbances in the power supply,

iii) response to pulse changes in the output resistance.

To gain some further insight into the behaviour of the converter, and motivate the need for closed–loop control, we also present the responses of the open–loop system.

Unless indicated otherwise, in all the experiments we consider as desired output voltage the value $V_d = 20$ Volts. This corresponds to a desired inductor current $\frac{V_d^2}{RE} = 0.4$ Amp. and to an equivalent duty ratio $\bar{\mu} = 1 - \frac{E}{V_d} = 0.5$.

6.1 Response to output voltage references

Step references

In fig. 5 we show the typical behaviour of the *open loop* system introducing a step in the duty ratio μ of 0.5. As we can see, the behaviour of the output voltage x_2 is quite good, it's fast and not to oscillatory. On the other hand, the current in the inductance x_1 has a very large overshoot that exceeds the limit of current available in the power source for a considerable time. This behaviour is not desirable because it could trigger the security elements that would disable the power source. We also observe that there exists a small undershoot due to the nonminimum phase characteristic of the system.

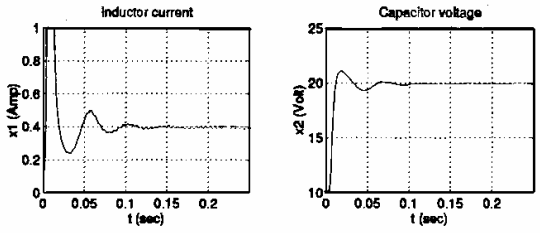

Figure 5: Open loop step response

In fig 6 we show a family of step responses of the system under **LAC** for different locations of the closed–lop poles of the linearized system. As expected, for faster poles we obtained faster responses. However, due to the presence of nonlinearities, specially the saturation of the inductor current, the time responses do not correspond to the pole placement proposed. In particular, the response of x_2 is quite sluggish, and we can not obtain oscillatory responses that are predicted by the linear approximation theory. The former can be explained via a simple root locus analysis which reveals that for large k_1 one pole approaches -20 while the other goes to $-\infty$, so the time response is dominated by the slowest pole. We also observed that for relatively small gains a significant steady state error appears, while the undershoot amplitude increases for faster responses.

In fig. 7 typical responses of the system under **FLC** for different values of a_1 and a_2 are presented. These corresponds to different pole locations of the closed–loop system described in the coordinates $[H,\ \dot{H}]$. Again, faster responses in x_2 are obtained with faster poles, which yields in it's turn higger peaks in x_1, being the speed of convergence of x_2 limited by the saturation. Notice, however, that for comparable convergence rates there is a significant reduction on the peak size with respect to **LAC**.

In fig. 8 we show the responses of the **PBC** for different values of R_1. From the plots we see that R_1, which is the sole design parameter, affects only the behaviour of x_1, while x_2 remains almost invariant.

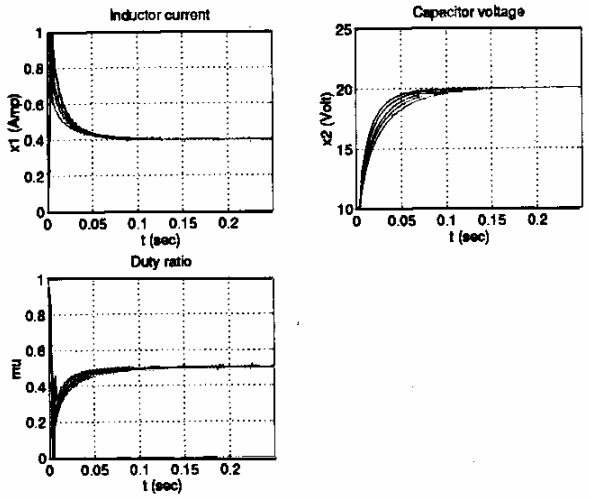

Figure 6: Step responses for **LAC**

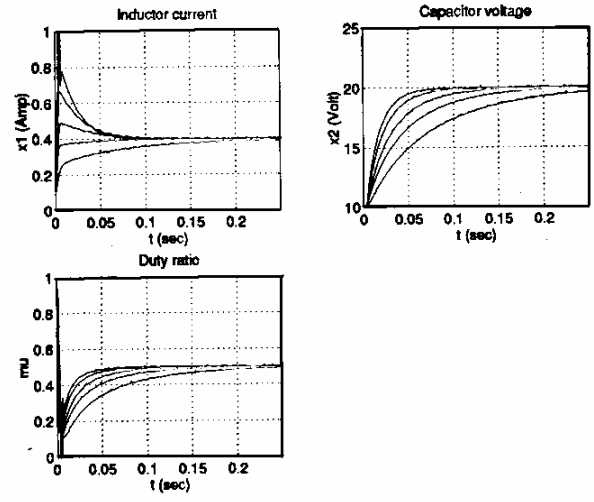

Figure 7: Step responses for **FLC**

Actually what happens is that for small damping x_1 is very slow with a large overshoot, as we increase the damping x_1 converges faster –with no overshoot–, finally at very large values it exhibits a fast peaking. As explained in section 3.1 damping determines the speed of convergence of x_2 towards z_{2d}, the wiggled responses in fig. 8 corresponding to small damping. However, z_{2d} remains essentially invariant to R_1. We should note that the peaking in z_{2d} predicted by the theory was not observed, we believe because it is filtered by the dominant pole.

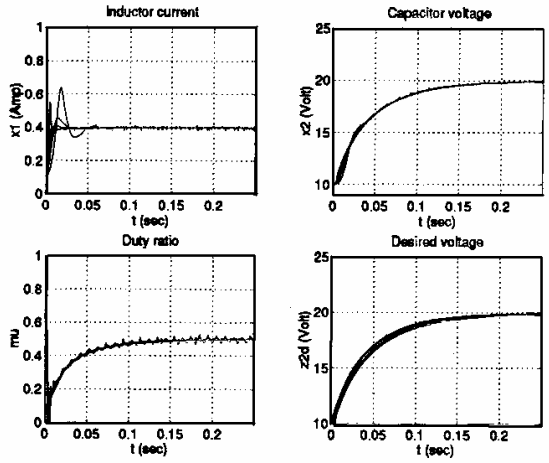

Figure 8: Step responses for PBC

In fig. 9 we present the response of the system with **SMC**. As we see, the sliding regime is reached almost instantaneously, thus x_1 reaches its desired value very fast. From the equations describing the sliding dynamics (26) we know that the response of x_2 is governed by the natural time constant $\frac{2}{RC}$, which makes slow this response. Notice that there are no tuning parameters in this control law.

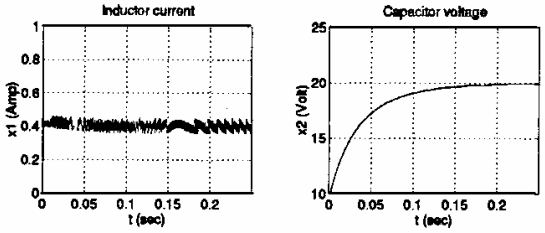

Figure 9: Step response for **SMC**

In fig. 10 we present the response of **SM+PBC** for different values of the design parameter R_1. Again, as in **PBC**, x_2 and x_{2d} remain almost invariant. Only x_1 and x_{1d} change, both exhibit a peak during the transient that becomes higger for bigger R_1..

Our conclusion of this subsection is that only **LAC** and **FLC** provide some flexibility to shape the step response. Two important advantages of **FLC** over **LAC** is that it achieves the same convergence rates with smaller inductor currents –hence less energy consumption–. Further the steady–state error was systematically smaller. As expected, the predictions of the theory are accurate only up to the point that the saturation levels (which is an unmodelled nonlinearity) are reached. We tend to believe that faster responses without saturation are not possible.

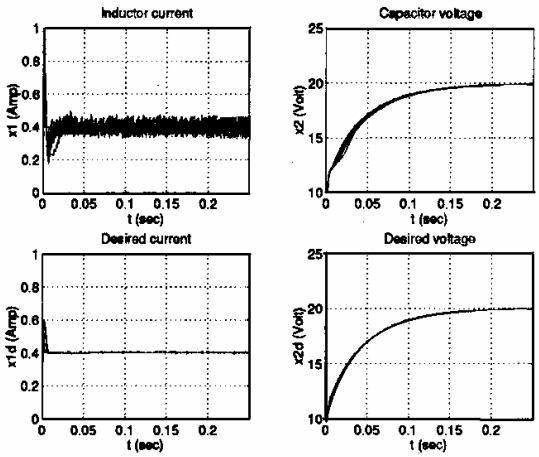

Figure 10: Step responses for**SM+PBC**

Sinusoidal references

Eventhough the controllers are designed for a regulation objective a very important characteristic to study in this system is its ability to try to follow a time varying desired output signal V_d. Obviously, this characteristic is closely related with its frequency response, and specifically with its bandwidth. In fig. 11 we show the closed–loop frequency responses for the five control laws. For reasons of physical construction of the system we can only follow reference signals of the form $V_d = V_{d0} + A_{Vd} sin(2\pi ft) > E$. The frequency responses were obtained asuming we are placed in the equilibrium point caused by the dc-component $V_{d0} = 20$ Volt and then we take only the alternating part of the response. To generate the gain plot we divide the amplitude of this alternating output signal betwen the ampliude $A_{Vd} = 5$ Volt for each frequency.

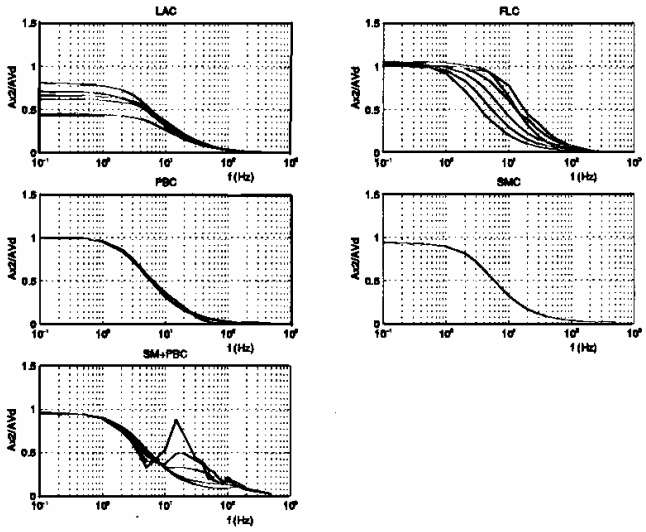

Figure 11: Frequency responses to periodic reference voltage, $\delta V_d(t) \mapsto \delta x_2(t)$

In **LAC**, we observe that there appears a problem of steady state gain, that is, for higger values of k_1, for instance $k_1 = 2.5, k_2 = 0.01$, the steady state gain almost reach 1 which is the spected value, but wich corresponds to a bandwith of 6 Hz. On the contrary, for lower values of k_1, for instance $k_1 = 0.5, k_2 = 0$,

the steady state gain decreases to 0.4615 with a bandwith of 20 Hz. This problem is due to the fact that the system has been linearized arround an equilibrium point, and now we are carrying the system far from this point putting in evidence its nonlinearities that are not considered in the control law.

In the case of **FLC** there is no problem of variations in the steady state gain and in this case the bandwidth can be enlarged choosing a_1 and a_2 such that the corresponding damping coeficient is small and the natural frequency high. For example, chosing $a_1 = 60, a_2 = 3600$ we have a bandwidth of 10.5 Hz and for $a_1 = 90, a_2 = 900$ we get a bandwidth of 2 Hz.

In **PBC** this frequency response is not afected when R_1 is changed, so the bandwith is fixed to 3.1 Hz. This is also the case for **SMC**. For **SM+PBC** the bandwith varies slightly depending on the value of R_1, for an $R_1 = 50$ we can enlarge the bandwith to 3 Hz, and for $R_1 = 5$ we reduce it to 2.1 Hz. We have observed also some resonance phenomena in the circuit for low values of R_1, this is manifested in the form of peaks in the frequency response which dissapear for higger values of R_1. We do not have at this point a physical or theoretical explanation of this phenomenon.

The results of these experiments are summarized in the table below.

Strategy	Cut-off frequency range (Hz)
LAC	****
FLC	[2.0, 10.5]
PBC	3.1
SMC	3.0
SM+PBC	[2.1, 3]

Besides the bandwidth we are, of course, also interested in the phase shift introduced in the loop. To assess this characteristic we show in fig. 12 some typical time responses of the output voltage for the various control strategies and a reference signal of 2Hz. We have chosen the tuning that gives the largest bandwidht. We can see that the smallest phase shift is achieved with **FLC**, which also provides the best achievable bandwidth. We should underscore the poor performance of **LAC** in this respect.

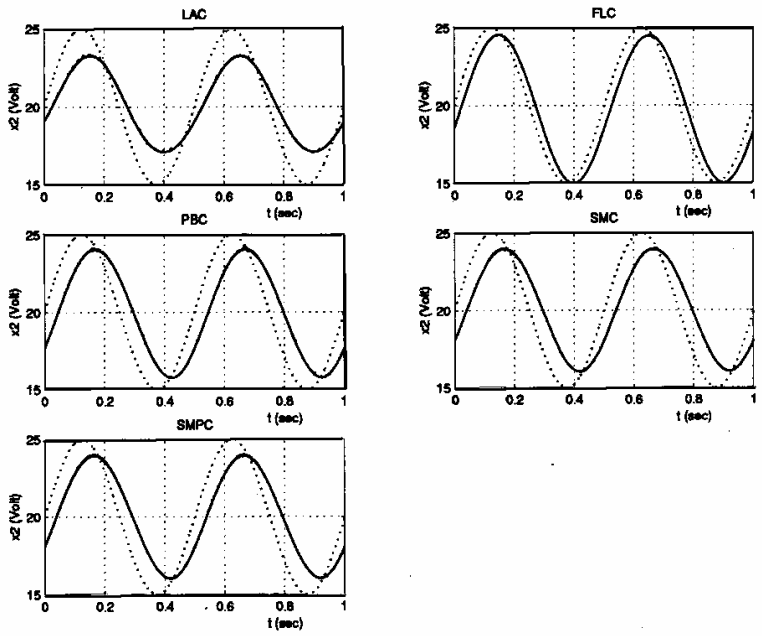

Figure 12: Time responses to a periodic reference signal $V_d(t)$

6.2 Disturbance attenuation

In this section we study the behaviour of the control laws in the face of a disturbance in the power supply. We consider two classes of disturbances steps and sinusoids.

Step disturbance

In this experiment we propose to add a pulse disturbance w to the power supply (obtained from a signal generator) of amplitude 3 Volts and duration 0.1 sec. In fig. 13 we show the behaviour of the output voltage x_2 for each control law and different tunings.

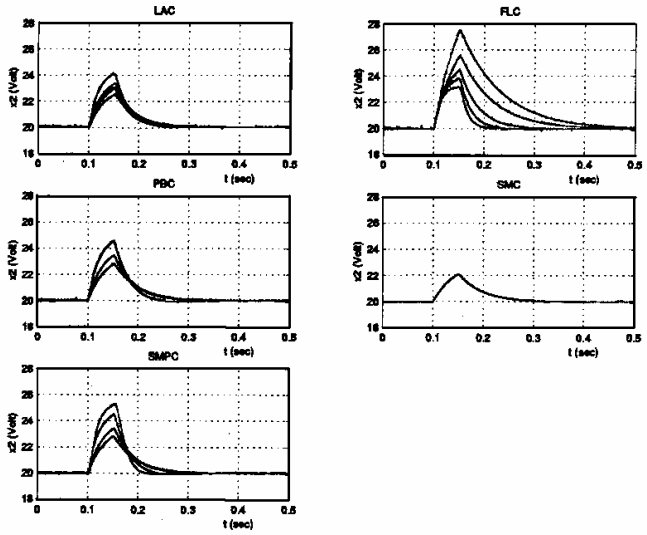

Figure 13: Response to a pulse disturbance $w(t)$

We can see that **FLC** is quite sensitive to step disturbances, while **SMC** is almost insensitive to it. To obtain some quantitative measure we evaluated the energy amplification of the circuit, that is we calculated the ratio

$$\gamma = \frac{||\tilde{x}_2||_2}{||w||_2} = \frac{||\tilde{x}_2||_2}{3\sqrt{0.1}}$$

where $\|\cdot\|_2^2 := \int_0^\infty (\cdot)^2 dt$. This number provides a lower bound to the $\mathcal{L}_2$-gain of the operator $T_{w\tilde{x}_2} : w \mapsto \tilde{x}_2$. See [10] for some theoretical evaluation of bounds on this norm for **FLC** and **PBC**.

In **LAC**, γ can be reduced using higger values of k_1 which implies that the dominant pole is slow, so for a $\gamma = 0.9059$ we have chosen $k_1 = 2.5$ and $k_2 = 0.01$ which results in a dominant pole near 20.

In **FLC**, γ can be reduced proposing high values of a_2 and small values of a_1, this corresponds to poles with high real and imaginary parts and damping coefficients less than 1.

In **PBC**, big values of R_1 reduce γ, for instance, a value of $R_1 = 50$ corresponds to a $\gamma = 0.4738$. This is consistent with the theoretical results reported in [10]. The same behaviour was observed for **SM+PBC**. For example, taking $R_1 = 50$ we obtain a $\gamma = 0.6409$.

The range of the gains that we obtained in our experiments is summarized in the table below.

Strategy	Ranges of γ
LAC	[0.5715, 0.9059]
FLC	[0.6855, 1.9787]
PBC	[0.6506, 0.9910]
SMC	0.4738
SM+PBC	[0.6409, 1.602]

Sinusoidal disturbances

In these experiments we obtain the frequency responses of the output voltage under periodic perturbations introduced in the power supply. To this end, we add to the voltage source E a perturbation $w = A_w sin(2\pi ft)$ where $A_w = 3$ Volts and we scan diferent values of f.

The magnitudes of the Bode plots ($w \mapsto \tilde{x}_2$) for the open loop system and those of the controllers (for different tuning parameters) are given in fig. 14. We see that in all cases the closed–loop behaves like a low pass filter and the question is what is the effect of the tuning gains on the steady-state gains and on the bandwidth and roll–off of the frequency responses.

Note that in these courves for each controller, variations in the parameters imply variations in both, steady state gain and cut-off frequency. Of course the best curve is that with the minimum steady state gain and cut-off frequency.

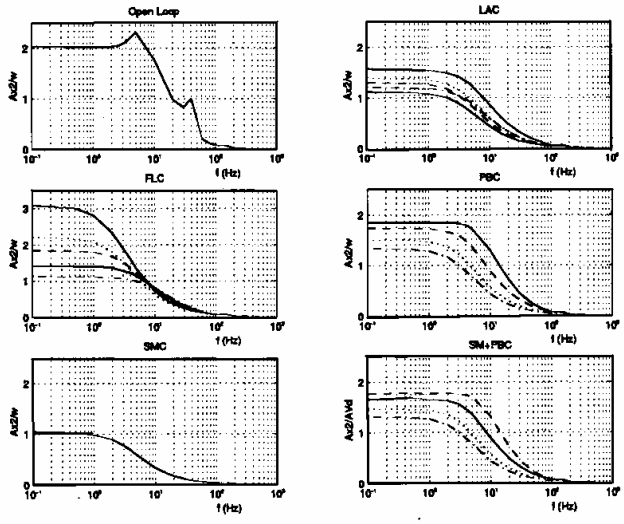

Figure 14: Magnitude Bode plots ($w \mapsto \tilde{x}_2$)

In open loop the cut–off frequency is of 14Hz, hence extremely bad disturbance attenuation. For the **LAC** controller, the steady state gain can be reduced if the gain k_1 is decreased, this corresponds also to a very small increasing in the cut-off frequency. For high values of k_1 and k_2 ($k_1 = 2.5, k_2 = 0.01$) the steady state gain could arrive up to 1.5625 with 10 Hz of cut-off frequency and for smaller values ($k_1 = 0.5, k_2 = 0$) this gain is 1.125 with 10.1 Hz of cut-off frequency.

In the case of **FLC** controller, depending on the pole locations, we can have steady state gains that go from 1.16 for fast poles ($a_1 = 60, a_2 = 3600$) until 3.1 for a dominant slow pole ($a_1 = 120, a_2 = 1600$). These pole locations correspond to cut-off frequencies of 14 Hz and 2.4 Hz respectively. Thus appearing a compromise between steady-state gain and cut-off frequency depending on the pole locations.

For **PBC** we have smaller steady-state gain and cut-off frequency for bigger values of R_1. For instance, a steady-state gain of 1.3775 with a cut-off frequency of 7 Hz, correspond to an $R_1 = 50$. And for an $R_1 = 5$, the corresponding values are 1.875, 10.1 Hz.

In **SMC**, since there is no design parameter, the steady-state gain and the cut-off frequency are unique and they take reaspectively the values 1.06 and 10 Hz . Wich means that disturbance rejection in this controller is quite good. For **SM+PBC**, as in the case of **PBC**, we have smaller steady-state and cut-off frequencies for bigger values of R_1. For instance, with an $R_1 = 5$ we have an steady-state gain of 1.3125 and a cut-off frequency of 7 Hz, and for $R_1 = 50$ we have 1.75 and 10.2 Hz, respectively.

In the following table we show the steady-state gain and cut-off frequency ranges we obtained experimentally for each control strategy.

Strategy	Steady-state gain range	Cut-off frequency range (Hz)
Open loop	2	14
LAC	[1.5625, 1.125]	[10.0, 10.1]
FLC	[3.10, 1.16]	[2.4, 14.0]
PBC	[1.375, 1.875]	[7.0, 10.1]
SMC	1.06	10
SM+PBC	[1.3125, 1.75]	[7, 10.2]

It's important to remark that this cut–off frequencies are relatively small compared with the posible perturbations caused by the natural line frequency noise (50/60 Hz), so the rejection of this kind of natural perturbations is assured.

6.3 Robutness to load uncertainty

In this experiment we introduce a load change that reduces the effective resistance from its nominal value of $R = 100\Omega$ to $R + \Delta R = 50\Omega$ during the interval $[0.5, 1]$ sec. To implement this effect a digital signal generated in a DSpace card is sended to the gate of a MOSFET transistor to turn it on or off. This transistor is actuating as a switch that connects or disconnects a resistance of 100 Ω placed in parallel with the nominal load, which is also of 100 Ω.

The open–loop response is shown in fig. 15. As we can see, there appears a steady state error in the voltage output x_2, that even if it's small, there is no way to reduce it.

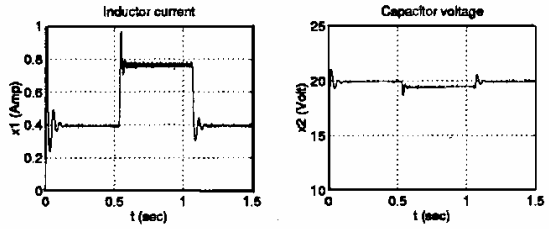

Figure 15: Open–loop response to a step change in the output resistance

As discussed in section 4 the fact that all control strategies are indirect makes them extremely sensitive to this kind of disturbance, introducing in particular a large steady–state error. To remove this error we tried an heuristic approach of adding an integral loop around the output voltage error (for continuous control laws) as well as the adaptive versions reported in section 4. Notice that we do not dispose of an adaptive scheme for **FLC**, however for simple step changes in the load the integral action corrected the steady–state error. It is an interesting open question how to provide **FLC** with adaptation capabilities to track time–varying parameters, as done for **PBC**.

Non adaptive versions

We show in fig. 16 the behaviour of the output voltage signal x_2 of the system been controlled for each strategy when there appears a pulse change in the output resistance, which is clearly unadmissible.

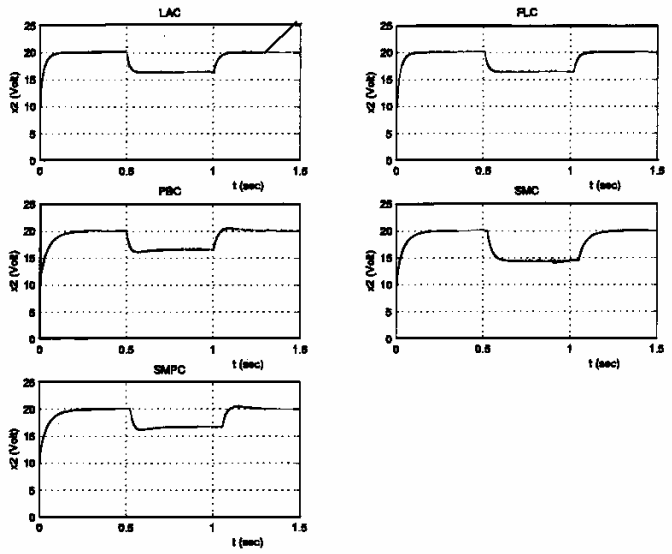

Figure 16: Output voltage behaviour for a disturbance in the output resistance

Adaptive versions

The adaptive version of **PBC** described in (33) with $\gamma = 1$ and $R_1 =$?? is shown in fig. ??. Observe that the parameter estimate converges very close to the true values, i.e. 0.1 and 0.2 Ω^{-1} (remember that the algorithm estimates $\frac{1}{R}$), but that this small discrepancy induces an steady state error both in the inductor current (which should be $\bar{x}_1 = 0.8$ for the new load resistance) and the output voltage. The error however vanishes when we come back to the nominal resistance, where now the estimate exactly converges to the true value. Given the proof of asymptotic stability of the desired equilibrium, the existence of this steady–state error for higher currents is particularly distressing. The only explanation we have is that since more current is passing through the electronic elements their parasitic losses become more significant. It may also be that the additional computations demanded by the adaptation law induce numerical errors. This critical issue of numerical sensitivity has been already observed in our work on control of induction motors [7].

As usual in adaptive control, eventhough we started the experiment with the right value of the load resistance, the estimate moves initially away from it. This in some way speed–up the step response of the output voltage.

For adaptive **SMC** we take again $\gamma = 1$ and observe the same phenomenon of lack of parameter convergence when the load is reduced. In this case, however, there is no steady state error in the output voltage, this because as we see from the ecuations, adaptation introduces an integral term in the output voltage error. The inductor current exhibits very high frequency components due to the low frequency used to generate the switching signal u.

In **SM+PBC** we took again $\gamma = 1$ and observed a behaviour very similar to **PBC**, with the addition of the high frequency oscillations in the current mentioned above.

Adding an integral term

In fig. 20 – 22 we present for the three laws employing a PWM, **LAC**, **FLC** and **PBC**, the responses to a pulse disturbance in the output resistance. In all cases the steady state error vanishes in a relatively short time with small overshoot. There is however some degradation in the quality of the first step response, a large overshoot, that could not be reduced via tuning without seriously degrading the transient and steady–state performances.

It is worth noting the oscillatory behaviour of **LAC** and **PBC** for both load values. To dampen the

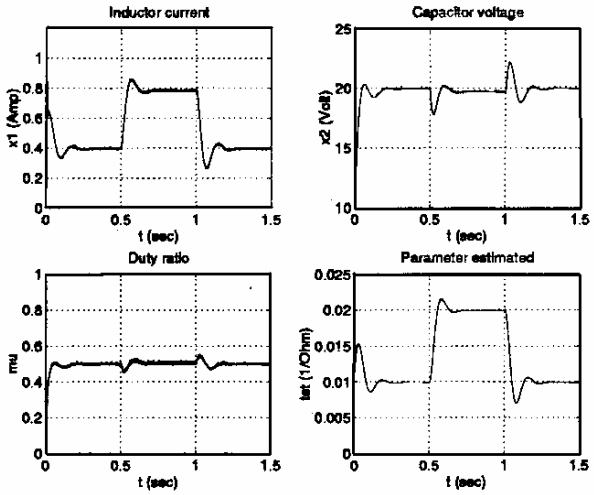

Figure 17: Response to a pulse disturbance in the output resistance for adaptive **PBC**

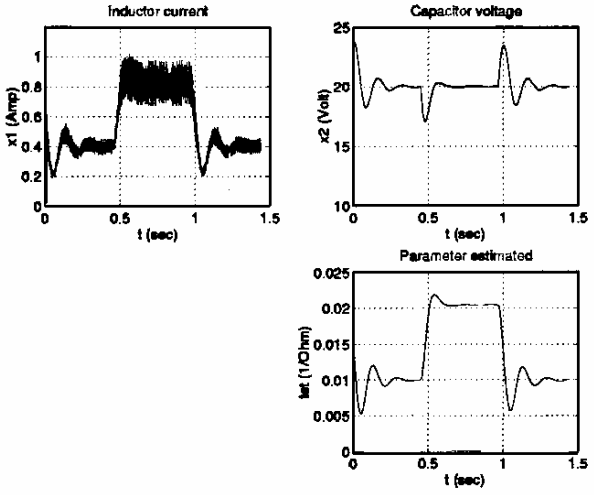

Figure 18: Response to a pulse disturbance in the output resistance for adaptive **SMC**

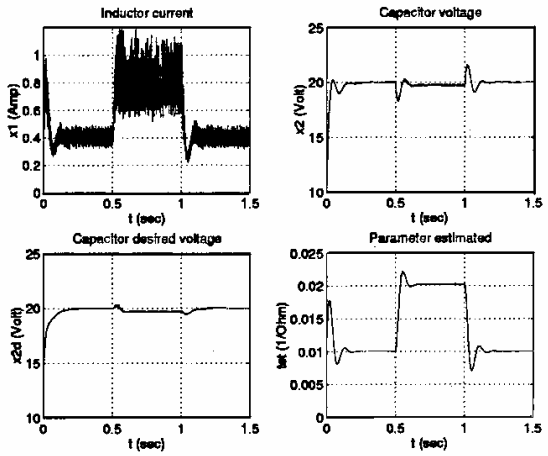

Figure 19: Response to disturbance in the output resistance for adaptive **SM+PBC**

oscillations the integral term had to be considerably reduced with the ensuing increase in the settling time. While for **PBC** this destabilizing effect of the integral action is not a serious problem, because we dispose of an adaptive version, for **LAC** it casts some doubts for its practical application.

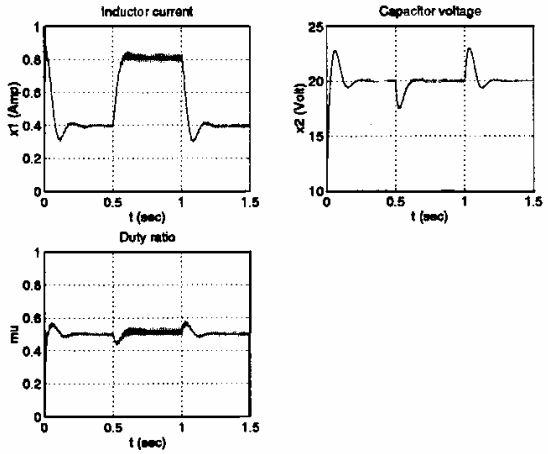

Figure 20: Response to a disturbance in the output resistance for **LAC** + Integral term

7 Conclusions

The following conclusions of our experimental study are in order:

- Nonlinear designs provide a promising alternative to classical lead–lag controllers. In particular **LAC** performed very badly in tracking time–varying references, and exhibited an undesirable oscillation when an integral term was added to compensate for load uncertainty.
- **FLC** performed very well in output regulation and tracking but exhibited a higher sensitivity to voltage disturbances than the other schemes. Incorporating an integral action effectively compensated for a step change in load resistance, eventhough no theory is available to sustantiate this. To handle other

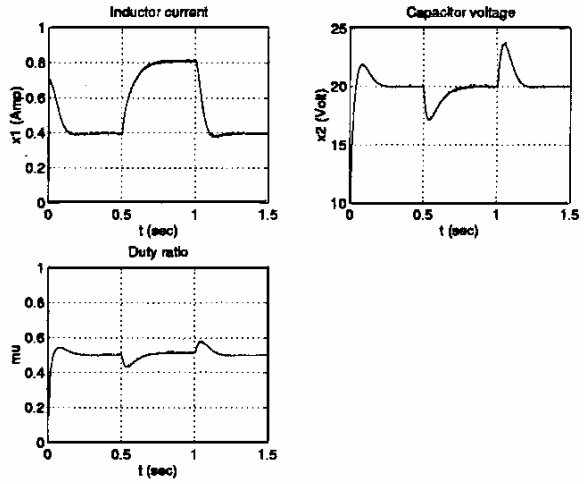

Figure 21: Response to a disturbance in the output resistance for **FLC** + Integral term

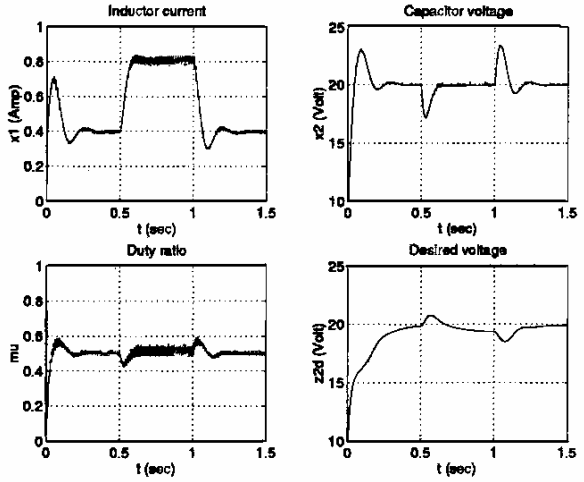

Figure 22: Response to a disturbance in the output resistance for PBC + Integral term

type of load changes (e.g., slowly time varying) the integral action will not be sufficient and some kind of adaptation should be incoporated into the controller.

- The main drawback of **PBC**, which is shared also by **SMC** and **SM+PBC**, is the inability to shape the output response, which evolves according to the open–loop dynamics. This, of course, stems from the fact that we cannot inject damping to the voltage subsystem without nonlinearity cancellation. On the other hand, **PBC** achieved a better disturbance attenuation, hence it may be a viable candidate for applications where rise time is not of prime concern. We should stress that, as shown in motor control, this is not a limitation intrinsic to passivity–based designs, rather it pertains to our ability to inject (pervasive) damping to the controlled variable.

- **SMC** and **SM+PBC** proved very robust to source disturbances but highly sensitive to parameter uncertainty. The latter could be alleviated incorporating a novel adaptation mechanism. The lack of flexibility of **SMC** is somehow alleviated in **SM+PBC**, at least to shape the disturbance attenuation characteristic. Unfortunately, both schemes suffer from the main drawback mentioned above.

- We can conclude our study stating that all of the algorithms were easy to implement in our Dspace–based facility. In contrast to the study carried out in [7] we were not interested here in issues pertaining to numerical sensitivity and computational complexity, this might prove important in a low–cost implementation.

References

[1] BOSE, B.K., *Modern Power Electronics: Evolution, Technology and Applications*, New York: IEEE Press, 1992.

[2] M. FLIESS, "Generalized controller canonical forms for linear and nonlinear dynamics," *IEEE Transactions on Automatic Control* Vol.. **AC–35**, pp. 994-1001, 1990.

[3] J. FREUDENBERG AND D. LOOZE, "Right half plane poles and zeros and design trade-offs in feedback design", *IEEE Transactions on Automatic Control*, Vol. 30, pp. 555-565, 1985.

[4] HULIEHEL F., B. YAAKOV "Low-frequency sampled-data models of switched moode DC-DC converters" *IEEE Transactions on Power Electronics*, Vol. 6, No. 1, pp. 55-61, jan. 1992.

[5] ISIDORI, A., *Nonlinear Control Systems*, 3rd. Ed. Springer-Verlag, London 1995.

[6] KASSAKIAN J.G., M. SCHLECHT, , AND G.C. VERGHESE, *Principles of Power Electronics*, Reading, Mass.: Addison-Wesley, 1991.

[7] K. KIM, R. ORTEGA, A. CHARARA AND J. P. VILAIN, "Theoretical and experimental comparison of two nonlinear controllers for current-fed induction motors", *IEEE Trans. Cont. Syst. Techn.*, (to appear).

[8] LEÓN DE LA BARRA B.A., "On undershoot in SISO systems", *IEEE Transactions on Automatic Control*, Vol. 39, No. 3, March 1994.

[9] MIDDLEBROOK R. D. AND S. CÚK, "A General Unified Approach to Modelling Switching–Converter Power Stages", *IEEE Power Electronics Specialists Conference*, (PESC), pp. 18–34, 1976.

[10] SCHERPEN J., R. ORTEGA, "On nonlinear Control of Euler-Lagrange Systems: Disturbance Attenuation Properties", (to appear in SCL)

[11] SIRA–RAMÍREZ H. AND P. LISCHINSKY–ARENAS, " The Differential Algebraic Approach in Nonlinear Dynamical Compensator Design for DC-to-DC Power Converters", *International J. of Control*, Vol. 54, No. 1, pp. 111-134, 1991.

[12] SIRA–RAMÍREZ H. "Sliding Motions in Bilinear Switched Networks", *IEEE Transactions on Circuits and Systems*, **CAS-34**, No. 8, pp. 919-933, 1987.

[13] SIRA–RAMÍREZ, H., R. ORTEGA, M. PÉREZ MORENO AND M. GARCÍA–ESTEBAN, "Passivity–Based Controllers for the Stabilization of DC–to–DC Power Converters", *Proc 34th IEEE CDC*, New Orleans, Dec. 13–15, 1995. (Also to be published in *Automatica*).

[14] H. SIRA, G. ESCOBAR AND R. ORTEGA, "On passivity–based sliding mode control of switched dc–to–dc power converters", *35th IEEE Conf. Decision and Control*, Kobe, Japan, Dec. 13-15 1996.

[15] ORTEGA R. AND SIRA-RAMÍREZ H., "Adaptive passivity-based control for multivariable DC to DC power converters of the Boost type" (Under preparation)

[16] ZEIN I., *Power converters laws: An experimental comparative study. DEA Report UTC* Compiègne, France, 1996.